Investigation of Charge Transport in Thin, Doped Sexithiophene Crystals by Conducting Probe Atomic Force Microscopy

Michael J. Loiacono, Eric L. Granstrom, and C. Daniel Frisbie*

Department of Chemical Engineering and Materials Science, University of Minnesota, 421 Washington Avenue SE, Minneapolis, Minnesota 55455

Received: October 8, 1997; In Final Form: January 5, 1998

Conducting probe atomic force microscopy (CPAFM) was used to measure the electrical transport characteristics of 2−14 nm thick doped crystallites of the organic semiconductor sexithiophene (6T) grown on Au and SiO_2 substrates by vacuum sublimation. To make the measurements, an AFM was modified to allow in situ switching from tapping mode imaging to point contact electrical characterization with an Au-coated tip. The crystals were characterized structurally by molecular contrast AFM imaging and consist of layers of 6T molecules oriented with their long axes nearly perpendicular to the substrate. For crystals grown on Au substrates, transport is probed through the thickness of the crystals (i.e., the vertical direction) using a CPAFM tip and the substrate as electrical contacts. On SiO_2 substrates, transport is measured parallel to the substrate between the CPAFM tip and a nanofabricated Au electrode in contact with the crystallite. The measurements on Au reveal an unexpected dependence of the conductance on crystallite thickness, namely that conductance is greatest for crystals that are three 6T layers thick, not one layer. Both the vertical and horizontal conductance measurements show nonohmic behavior which may arise from an energy barrier to charge injection at the Au−6T interface. The reproducibility of the CPAFM methodology for probing transport in these extremely thin organic crystals and the observation of nonohmic behavior underscore the importance of nanoscale transport measurements afforded by CPAFM.

Introduction

The possibility of low-cost, mechanically flexible electronics for flat-panel displays and smart cards motivates current efforts to fabricate transistors, light-emitting diodes (LEDs), and lasers from organic materials.[1] These efforts build upon 40 years of research on charge transport and luminescence in organic semiconductors.[2] However, continued progress will depend on everincreasing comprehension of factors that affect carrier mobility in these materials, such as electronic structure, carrier trapping, delocalization, and charge injection barriers.[3] Many recent transport measurements on organic semiconductors have been performed on polycrystalline films over length scales of 1 μm or greater, meaning that the measured transport characteristics reflect average film properties. An alternative strategy is to design experiments that probe transport over sub-100 nm length scales so that the transport properties can be correlated directly with specific, well-characterized supramolecular structures. Mesoscopic approaches have been very productive already in studies of inorganic semiconductors[4] and, when applied to organic materials, offer unprecedented opportunities to observe transport phenomena that are peculiar to organic mesostructures.

We describe here the use of a new technique, conducting probe atomic force microscopy (CPAFM), to measure the electrical transport characteristics of extremely thin, doped organic semiconductor crystallites. CPAFM is a powerful scanning probe method that combines nanoscale electrical characterization and topographic imaging by employing a metal-coated cantilever−tip assembly as both a scanning electrical contact and force sensor. Reported CPAFM studies include electrical measurements on individual carbon nanotubes,[5] resonant tunneling diodes,[6] and nanoscopic metallic contacts.[7] CPAFM is eminently suited to electrical characterization of small organic structures, having the advantage relative to scanning tunneling microscopy (STM)[8] that the current−voltage ($I-V$) relationship is decoupled from the sample position feedback mechanism. A broad variety of samples may be investigated, including those having regions with widely varying conductivities. Additionally, normal force sensing with a cantilever−tip assembly facilitates straightforward interpretation of the position of the tip relative to the organic material; that is, a measured repulsive force indicates intimate contact.

We have focused our initial CPAFM studies on crystallites of sexithiophene (6T), Scheme 1A. 6T is a p-type organic semiconductor that has been studied extensively in thin film transistor (TFT) experiments[9] because its hole mobility rivals that in amorphous Si, making it a viable candidate material for all-plastic TFT technology. It was the discovery[9m] of high hole mobility in 6T that rekindled efforts to develop organic semiconductors for transistor applications, and 6T currently represents an archetypal model of organic semiconductors. Our measurements are the first to probe transport in single 6T crystals over nanometer length scales, and we demonstrate that the transport has unexpected nonohmic dependence on crystal thickness. Further, we show that it is possible by CPAFM to measure directly the transport properties of organic crystals as thin as a single 6T monolayer. This establishes the technical feasibility of future experiments that probe details of transport

* Address correspondence to this author. E-mail: frisbie@cems.umn.edu.

S1089-5647(97)03269-0 CCC: $15.00
Published on Web 02/12/1998

SCHEME 1: (A) Monoclinic Unit Cell of 6T.[9h] (B) CPAFM Tip on a 2 ML 6T Crystal. (C) Configuration for the Vertical *I*−*V* Measurements. (D) Configuration for the Horizontal *I*−*V* Measurements

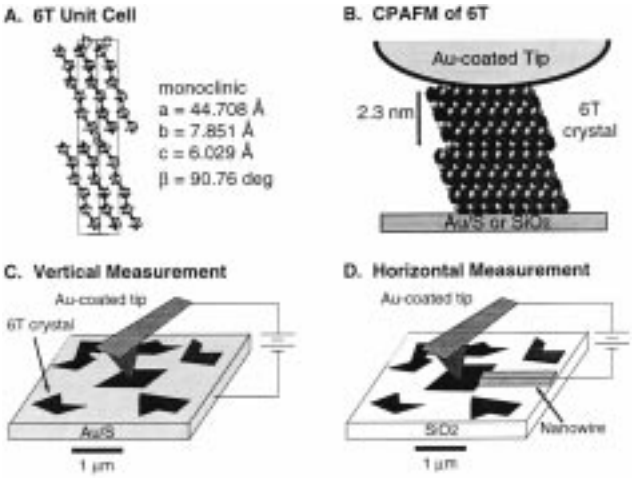

associated with metal−organic interfaces or specific nanostructures, such as individual defects or grain boundaries.

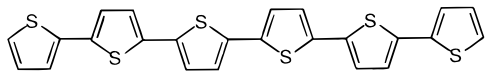

6T

The 6T crystals are grown on flat Au and SiO_2 substrates by vacuum sublimation and range from 1 to 6 monolayers (2−14 nm) in thickness and 2−5 μm in length and width. We probe charge transport through these crystals, after doping them with iodine, using two different CPAFM configurations. For the crystals grown on the conducting Au substrates, we measure transport through the thickness of the crystals, i.e. perpendicular to the substrate, Scheme 1B,C. In these perpendicular studies, the *I*−*V* characteristics are linear in the ±50 mV regime. Significantly, the perpendicular conductance (*I*/*V*) of the doped 6T crystals does not decrease monotonically with increasing thickness as might be expected, but instead has a maximum at 3 monolayers (ML) thickness, and we discuss the possible implications of this finding to charge injection at metal−organic interfaces. For crystals grown on insulating SiO_2 substrates, we measure the horizontal *I*−*V* characteristics, i.e., in the direction parallel to the substrate, of 6T crystals that are contacted at one end by a nanofabricated Au electrode, Scheme 1D. To obtain measurable currents in this configuration, we must scan a larger voltage range, and the resulting *I*−*V* traces are not linear, but rectifying. At fixed applied bias between the conductive CPAFM tip and the nanoelectrode, the conductance increases with increasing crystallite thickness and plateaus at 4 ML. We suggest that the observed thickness dependence is a result of charge injection into only one or two layers and the anisotropy of conduction within the crystal.

To facilitate reproducible electrical measurements and to increase the overall robustness of the CPAFM technique, we have developed a variation of CPAFM that allows interchange in situ between tapping and contact feedback modes. Specifically, we use tapping mode to image the 6T crystals and employ an operator-activated external circuit to switch to contact mode for point contact electrical characterization of a preselected crystal. After completion of the measurement, we deactivate the external circuit to return to tapping mode feedback. This procedure prevents damage to the 6T crystals and the metal-coated tips by avoiding the frictional wear associated with contact mode imaging and greatly enhances the practicality of this characterization method.

Experimental Method

Materials. Sexithiophene ($C_{24}H_{14}S_6$) was synthesized from terthiophene ($C_{12}H_8S_3$, Aldrich, Milwaukee, WI) using a previously reported literature procedure.[9g] Purification was accomplished by Soxhlet extraction with hot acetone and mesitylene, followed by three successive vacuum sublimations. Au (99.999%) and Cr (99.99%) were purchased from Mowry, Inc. (St. Paul, MN) and R. D. Mathes, respectively. Highly oriented pyrolytic graphite (HOPG) was obtained from Digital Instruments (Santa Barbara, CA), and polished, single-crystal Si wafers (⟨100⟩ orientation) were obtained from WaferNet (San Jose, CA). Solvents and NaSH were purchased from Aldrich.

Preparation of Conducting Probes. Rectangular Si cantilevers (120 μm long) with integrated tips (Digital Instruments, Santa Barbara, CA) were coated with 70 Å Cr followed by 700 Å Au by thermal evaporation at 10^{-6} Torr.

Preparation of Conducting Substrates. Flat Au substrates (mean roughness < 1 nm) were prepared using a previously reported templating procedure.[10] Briefly, 2000 Å of Au was deposited by thermal evaporation onto a heated mica sheet (300 °C) at 10^{-6} Torr. After cooling, the Au side of the Au-coated mica sheet was glued to a glass cover slip (∼1 cm diameter) with epoxy and left to cure at room temperature for 24 h. The mica was then cleaved off using a razor blade, exposing a smooth Au surface.

These Au substrates were immersed for 30 s in a 1 mM aqueous solution of NaSH (filtered). The purpose of this step was to coat the Au with a layer of S atoms (see Results). The presence of S on Au surfaces treated in this manner was verified by X-ray photoelectron spectroscopy (XPS).

Preparation of Insulating Substrates. SiO_2 layers 150 nm thick were grown on polished, single-crystal Si wafers by thermal oxidation. The SiO_2 had a mean roughness of <1 nm over a 5 μm × 5 μm area as determined by AFM. Electron beam lithography was used to pattern Au wires onto these oxidized wafers. After patterning the Au leads, the wafers were cleaned by exposure to a 400 W O_2 plasma for 2 min. The patterned wafers were then cut into 1 cm × 1 cm squares prior to deposition of 6T.

Deposition of 6T. Thin crystallites of 6T were grown on the S-treated Au substrates or on the SiO_2 substrates by vacuum sublimation at 10^{-4} Torr. The deposition was accomplished by ramping the temperature (∼1 °C/min) of a sand bath surrounding the bottom part of an evacuated glass sublimation vessel (volume ∼300 cm^3). The vessel was charged with a few grains of powdered 6T. When the sand temperature reached 260−280 °C, the sand bath was removed and the vessel allowed to cool. During this deposition process, the substrate temperature was maintained at ∼170 °C. The 6T crystals were subsequently doped by exposing them to I_2 vapor at room temperature for exactly 30 min.

Conducting Probe Atomic Force Microscopy. CPAFM was perfomed using a Digital Instruments Nanoscope III AFM. An Au-coated AFM probe was mounted in a glass cell designed for AFM tapping mode imaging under liquids. The purpose of using the glass tapping mode cell (instead of the more common metal version) was to electrically isolate the tip from the rest of the head. The metal spring clip that holds the cantilever substrate in place was used to make electrical contact to the

AFM probe. A second electrical contact was made to the sample substrate by connecting with silver paint a fine gauge wire to a conductive portion of the substrate; in the case of the flat Au substrates, the wire was bonded directly to the Au, and in the case of the SiO_2 substrates, the wire was bonded to the contact pads at the end of the lithographically patterned Au electrodes. The leads to the AFM probe and the substrate were connected to the terminals of a Keithley model 236 source measure unit.

The samples were imaged and characterized electrically in air. Imaging of the sample with conducting probe tips was accomplished using tapping mode feedback (constant amplitude). To make an electrical measurement, the scan size was dropped to 0 × 0 nm and the force calibration routine of the Nanoscope software was entered. The cantilever piezo drive amplitude was set to 0 V, which stopped the cantilever oscillation. From the deflection versus Z-position plots, the zero deflection setpoint voltage was determined. At this point, the microscope was switched into contact mode feedback using a home-built circuit external to the AFM controller (described below). The setpoint value was set to the zero deflection voltage plus 0.1 V to ensure a slight positive deflection of the cantilever (∼50 nN load). A current−voltage curve was recorded in about 2 min using the Keithley source-measure unit controlled by a Macintosh computer. To return to tapping mode imaging, the potential difference between the tip and substrate was set to 0 V via the source measure unit, and the entire feedback switching procedure described above was reversed. Reimaging the sample area typically showed no detectable damage as a result of the electrical measurement. In cases where damage (e.g., pitting) was observed, the $I-V$ data were not used.

The external circuit to switch the feedback modes is based on a noninverting differential amplifier. The inputs to the amplifier are the desired setpoint voltage (accessible via the ribbon cable connecting the microscope to the controller) and the deflection (A−B) voltage (also accessible on the ribbon cable). The amplified difference between the inputs is fed to the controller as the error signal, replacing the error signal that the microscope normally returns to the controller via the ribbon cable when in tapping mode.

Results

Characterization of 6T Crystals. Figure 1A,B shows AFM height images of microscopic 6T crystals grown on S-treated Au (referred to as Au/S) and clean SiO_2 substrates by vacuum sublimation. The crystals on both substrates typically range from 2 to 5 μm in length and width and 2−14 nm in thickness. We found that passivation of the flat Au substrates with S atoms (by exposure to aqueous NaSH) was helpful in growing discrete crystals reproducibly on Au surfaces. We chose pretreatment with S because of the known affinity of S for Au and intuition that a S-terminated surface would be chemically similar to SiO_2, and therefore likely to promote crystallite formation. Deposition of 6T on untreated Au surfaces often did not produce well-defined 6T structures possibly because strong interactions between S in 6T and the Au surface prevented surface diffusion. Importantly, the adsorbed S layer did not compromise measurably the conductivity of the Au substrate (see below), but the specific effects of the S pretreatment on electronic properties of the Au−6T contact are not clear and will have to be addressed in future investigations.

Our conclusion that the structures shown in Figure 1 are crystals of 6T is based on high-resolution AFM imaging, Figure 2, and comparison to the known crystal structure of the relevant

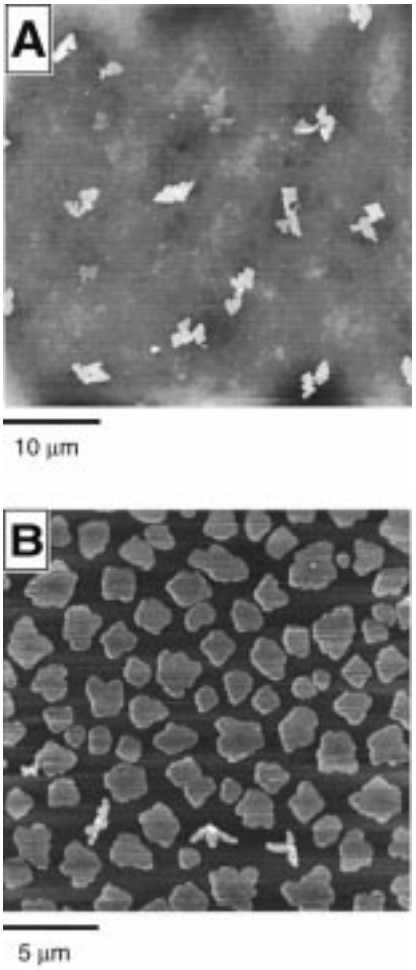

Figure 1. AFM height images of 6T crystals grown by vacuum sublimation onto Au/S (A) and SiO_2 substrates (B).

polymorph of 6T, Scheme 1A.[9h] The unit cell shown in Scheme 1A is monoclinic (a = 44.708 Å, b = 7.851 Å, c = 6.029 Å, β = 90.76°) with $P2_{1/n}$ symmetry. Within the *bc* planes of this structure, the molecules pack in the herringbone fashion typical of planar aromatic molecules and the long axis of the 6T molecules in these planes is tilted at 23.5° with respect to the *a* axis. The height image in Figure 2A shows an individual crystal with multiple terraces on an Au/S substrate. The terrace steps are 2.3 nm tall, as shown in the line scan in Figure 2B, corresponding to approximately half the value of the *a* parameter of the unit cell (Scheme 1A). The observed step height suggests that the terraces correspond to individual 6T monolayers (ML). Molecular resolution AFM imaging on top of a terrace, Figure 2C, confirms this assignment. In this image, we observe a surface lattice with 5.2 and 4.7 Å corrogation in the b' and c' directions, respectively (see Fourier analysis inset); the angle α between the b' and c' directions is 75°. The relationship of this measured lattice to the crystallographic unit cell parameters (b and c) is shown in the molecular model of the *bc* face in Figure 2D. Figure 2D is rotated so that the b' and c' directions correspond with those same directions in the AFM image in Figure 2C. Analysis of several crystals with different thicknesses gave average values of 5.0 ± 0.5 Å for b' and c' parameters, in close agreement with the calculated value of 4.9 Å for both of these directions based on the known unit cell parameters. The average α values of 75 ± 5° also matched the predicted value (75.9°), establishing that the 6T structures on Au/S substrates are crystals with the *bc* planes parallel to

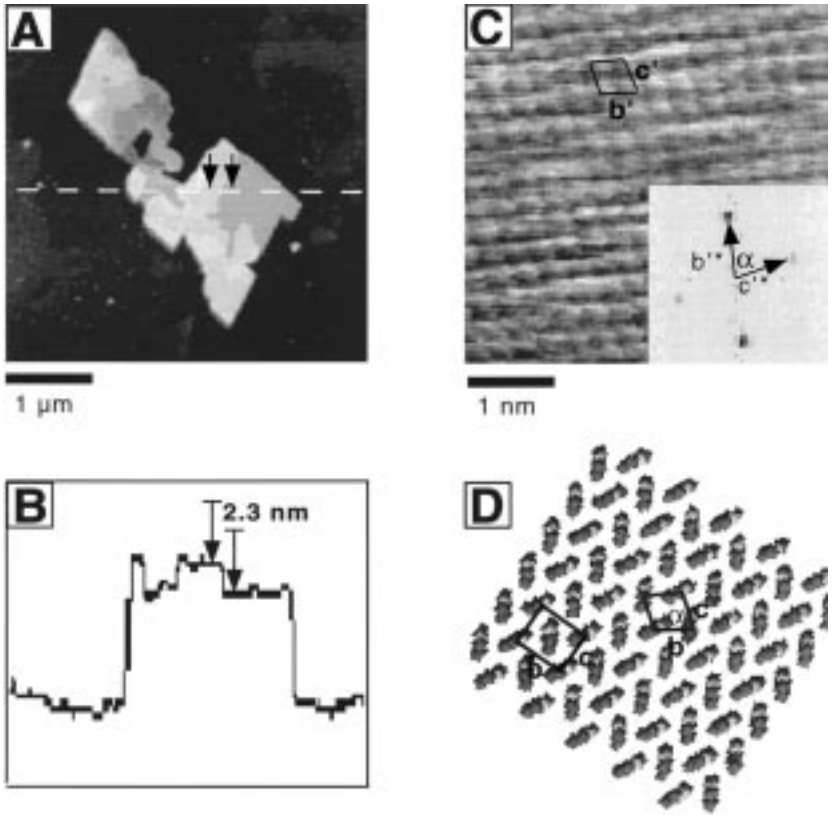

Figure 2. Structural characterization of 6T crystals. (A) AFM height image of a 6T crystal on Au/S showing multiple terraces. (B) Height profile along dashed line in A showing a 2.3 nm step. (C) Molecular contrast AFM image of 6T. The surface lattice parameters (b' and c') are overlayed on the image. The Fourier transform of the image shown in the inset was used to determine the magnitude of b', c', and α. (D) Model of the *bc* plane of 6T showing the observed surface lattice. The plane is rotated so that b' and c' shown in D are parallel with b' and c', respectively, in C.

the substrate, as shown in Scheme 1. For 6T on SiO_2, we observed different crystal shapes (compare parts A and B of Figure 1), but we obtained lattice parameters indistinguishable from those obtained for 6T on Au/S. Electron diffraction from polycrystalline 6T films on a variety of substrates has shown that the molecules are oriented with their long axes nearly perpendicular to the substrate.[9b,f] It is therefore not surprising that we found that the 6T crystallites grown on Au/S and SiO_2 substrates in this study had the lamellar structure depicted in Scheme 1 in which the molecules are slightly tilted with respect to the surface normal.

Exposure of 6T crystallites to I_2 vapor for 30 min produced no change in the lattice structure or morphology of the crystallites detectable by AFM. Since it is known that I_2 will intercalate into crystals of thiophene oligomers,[11] the absence of detectable structural changes indicates that the amount of I_2 that penetrated the crystals was very small, too little to result in detectable structural changes in lattice parameters, but adequate to increase electrical conductivity by several orders of magnitude. A calculation of carrier concentration in the doped crystals supports this conclusion (see Discussion).

Characterization of Conducting Probes. We characterized Au-coated AFM probes by scanning electron microscopy (SEM) and by recording $I-V$ traces for these probes in contact with graphite. Figure 3A,B shows SEM images of Au-coated probes at two different magnifications. From the images, it is evident that the Au coating is conformal and uniform. $I-V$ traces for an Au tip in contact with graphite as a function of applied load are shown in Figure 3C. For virtually all tips we tested (>20), we obtained linear $I-V$ curves between −10 and +10 mV. The conductance of a representative tip−graphite junction as a function of load force is shown in the inset. The conductance is $2 \times 10^{-6}\ \Omega^{-1}$ at 50 nN applied load and increases linearly until 250 nN load, at which point the tip deforms plastically. After plastic deformation, lowering the load does not lower the conductance appreciably. However, if the load is kept less than ∼200 nN, the load dependence of the $I-V$ traces is reproducible for most Au-coated tips. This is a remarkable result because we estimate the compressive stress at the tip under a 100 nN load is about an order of magnitude greater than the macroscopic yield stress of Au. Thomson and Moreland have reported similar findings,[7] and a detailed analysis of the conductance of tip−graphite junctions as a function of load is the subject of a separate investigation in our laboratory.[12]

The contact resistance of the Au-coated probes with the either Au or Au/S substrates was roughly 20 Ω at 50 nN load force. Because of the low resistance of the contact and the millivolt bias resolution of our source measure unit, attempts to record $I-V$ traces on naked Au or Au/S substrates resulted in extraordinarily high current densities (10^7 A/cm^2), which often destroyed the tip Au coating. We can conclude that the layer of S atoms does not appreciably alter the conductivity of the Au substrate.

CPAFM of 6T Crystals on Au/S Substrates. We probed the vertical (through thickness) conductance of 6T crystals grown on Au/S substrates using the experimental configuration in Scheme 1C. Figure 4 shows the $I-V$ trace between −50 and +50 mV for a 5 ML thick 6T crystal on Au/S after doping with I_2. We consistently observed linear $I-V$ traces for all doped crystals inside the ±50 mV window. The conductance ($I/V = 8 \times 10^{-10}\ \Omega^{-1}$) of the doped crystal associated with the trace in Figure 4 is at least 8000 times greater than the conductance of the same crystal before doping. Extremely low currents and poor signal-to-noise prevented us from measuring

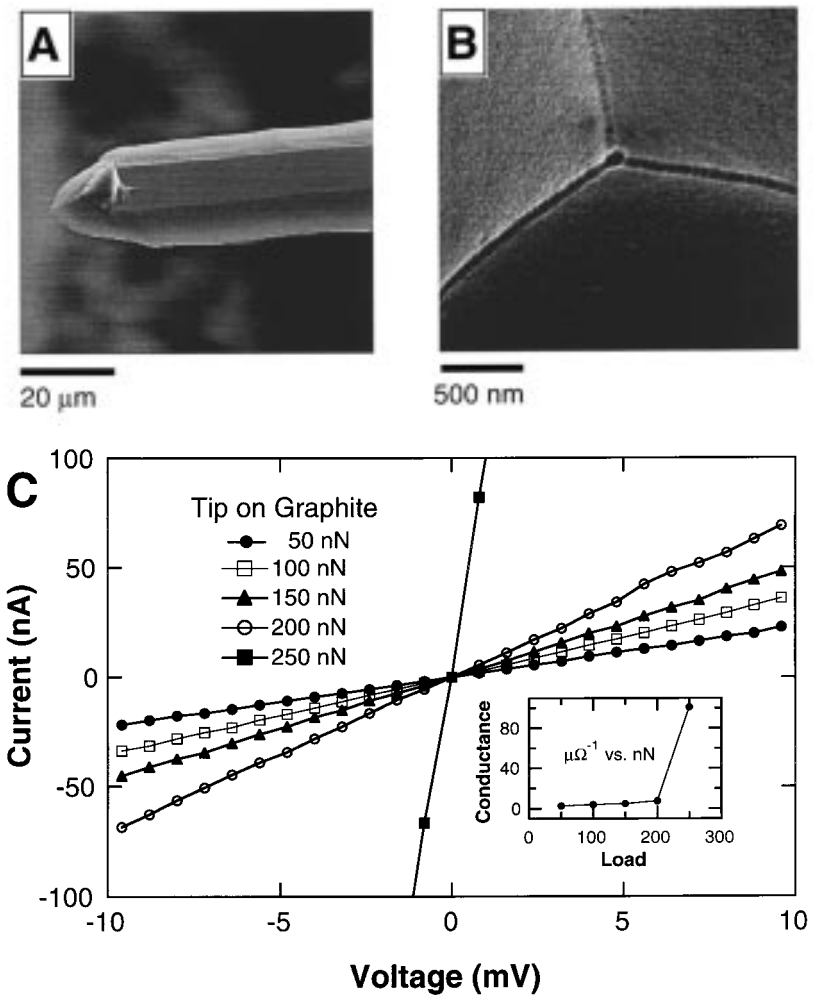

Figure 3. (A and B) SEM images of an Au-coated CPAFM tip. (C) Current−voltage characteristics of Au tips in contact with graphite as a function of compressive load. The inset shows conductance (*I*/*V*) vs load. The increase in conductance with increasing load is expected since the tip−graphite contact area will also increase with load. The large increase in conductance upon application of a 250 nN load is likely the result of plastic deformation of the Au coating, which significantly increases the tip−graphite contact area.

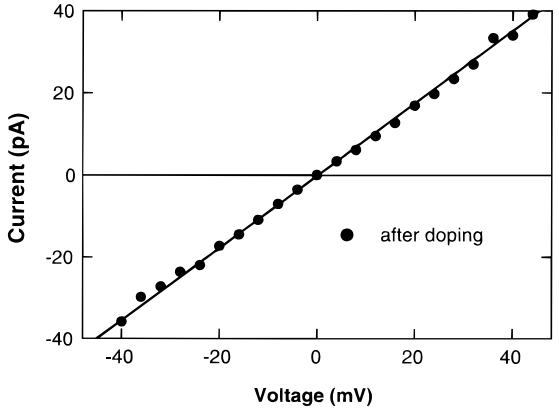

Figure 4. Point contact *I*−*V* trace of a 5 ML thick 6T crystal on Au/S after exposure to I_2 vapor for 30 min. The measurement was performed using the vertical configuration shown in Scheme 1C. Conductance (*I*/*V*) is 8×10^{-10} Ω^{-1}.

the conductance of *undoped* crystals over the ±50 mV regime. Therefore, the factor of 8000 is a lower limit to the conductance increase upon doping.

To determine the uniformity of doping in the 6T crystals, we measured I−V traces through a 6T crystal on an Au/S substrate at many different positions on the crystal, Figure 5A. The numbers in Figure 5A denote the positions where *I*−*V* traces were recorded with the conducting tip. Again, the observed traces were linear over the ±50 mV window at each of the nine positions. Figure 5B shows a plot of conductance versus the tip position. The key observation is that the conductance ($\sim 5 \times 10^{-10}$ Ω^{-1}) varies by less than a factor of 2 across the crystal. These results were reproduced on several crystals, indicating that there are not regions of these crystals that are inherently more conductive than other areas. The inference is that the dopant concentration is laterally uniform.

We chose six crystals of approximately equal area on Au/S substrates ranging in thickness from 1 to 6 ML and measured several *I*−*V* traces through each from −50 to +50 mV. The six crystals are shown in Figure 6, and representative *I*−*V* curves are shown in Figure 7A. Each trace in Figure 7A has an associated linear fit. The critical observation is best seen in Figure 7B, which shows conductance as a function of thickness, or number of ML. The plot shows a sharp peak in conductance at 3 ML (7×10^{-10} Ω^{-1}), with 1 and 2 ML crystals showing 600 and 30 times smaller conductance than the 3 ML crystal, respectively. The plot of resistance versus number of ML shown in the inset demonstrates that resistance increases linearly with thickness above 3 ML. The results in Figure 7 were very reproducible; the same peak in the conductance plot versus number of ML was observed for 1−6 ML crystals on each of three different Au/S substrates.

CPAFM of 6T Crystals on SiO_2 Substrates. We measured the lateral *I*−*V* characteristics of doped 6T crystals on SiO_2

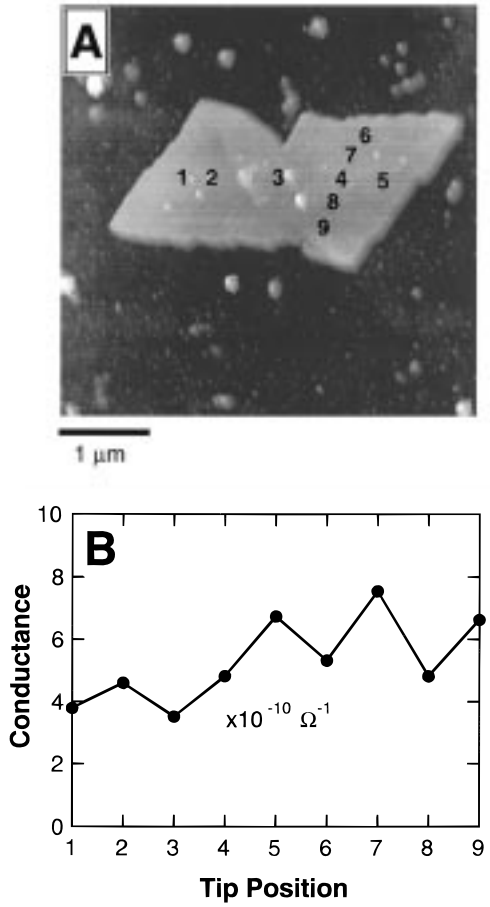

Figure 5. (A) AFM height image of a 5 ML 6T crystal on Au/S showing nine positions where the vertical (through thickness) conductance was measured using CPAFM. (B) Vertical conductance of the crystal in A as a function of tip positions shown in A.

substrates using the configuration shown in Scheme 1D. Figure 8 shows an AFM height image of a 6T crystal that grew off of a nanofabricated Au wire on SiO_2. $I-V$ traces of such crystals with different thicknesses were obtained by positioning the tip 100 nm from the Au wire. Figure 9A shows $I-V$ traces obtained for doped 6T crystals varying in thickness from 1 to 5 ML. Because the distance between electrodes (tip and nanowire) is much greater in these horizontal measurements than the vertical measurements, we scanned a larger voltage range, from −500 to +500 mV, to obtain measurable currents. The $I-V$ traces show strongly rectifying behavior; that is more current flows when the tip is biased positive than when it is biased negative. Conductance at a fixed tip−electrode bias of 500 mV is plotted versus the number of MLs in Figure 9B. As is evident in the figure, the conductance increases with thickness until 4 ML, at which it plateaus.

Discussion

Our demonstrated ability to measure electrical transport in sexithiophene crystals as thin as 1 ML hinged on finding means to contact the crystals without damaging them or the CPAFM probe. We have accomplished this by modifying previously reported CPAFM strategies to allow in situ switching between tapping mode imaging and point contact electrical characterization under constant deflection feedback. This combined tapping/contact mode approach substantially enhances the feasibility of CPAFM experiments on soft organic nanostructures and augments the already powerful imaging and electrical measurement combination previously reported.[5]

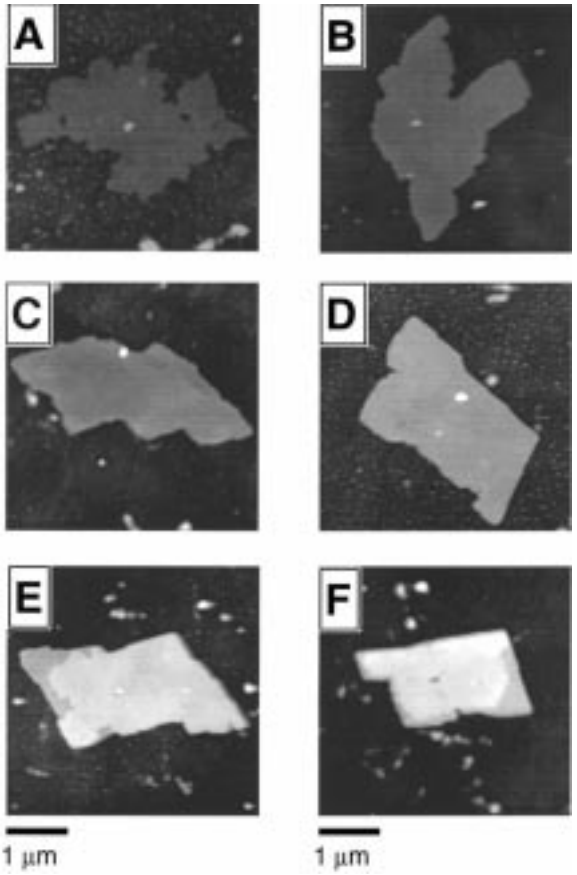

Figure 6. (A−F) AFM height images of 1 ML (2 nm), 2 ML (5 nm), 3 ML (7 nm), 4 ML (9 nm), 5 ML (12 nm), and 6 ML (14 nm) thick 6T crystals on Au/S, respectively.

Several specific observations can be made regarding our CPAFM methodology. First, we employed Au-coated tips for three reasons: (1) Au does not form a stable oxide; (2) it has a high work function (5.1 eV) facilitating hole injection into 6T; (3) it can be deposited conveniently on tips by thermal evaporation. Our microscope modification allowed us to use the same Au-coated tip for several hours, enough time to complete $I-V$ measurements on many individual 6T crystals. As long as the load force during the electrical measurements was kept less than ∼200 nN, $I-V$ measurements with the same tip were very reproducible over this several hour time frame.

Second, the large electric fields (∼10^5 V/cm) in our CPAFM experiments opened the possibility for complications due to electrolysis of adsorbed water, or other contaminants, and dielectric breakdown. If electrolysis had been a significant problem, the current would have swamped the variation in conductance associated with crystals of different thickness. Since we clearly observed a marked dependence of conductance on crystal thickness, it appears unlikely that electrolysis was important. Likewise, had breakdown been occurring, we would have observed strong time dependence of our $I-V$ traces due to decomposition of 6T, which we did not. The overall reproducibility and consistency of our data indicated that neither adsorbed contaminants nor strong fields compromised the measurements.

Third, we can make an estimate of typical tip−sample contact areas from our conductance measurements on naked Au substrates. Following Thomson and Moreland,[7]

$$R_c = \frac{4\rho l}{3\pi a_c^2}$$

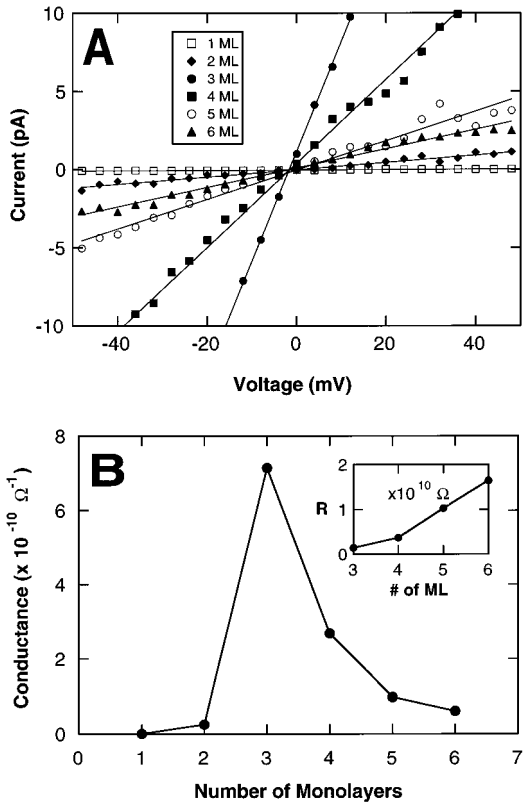

Figure 7. (A) Point contact $I-V$ characteristics of the 6T crystals on Au/S shown in Figure 6. Experimental configuration shown in Scheme 1C. (B) Vertical conductance (I/V) of the six crystals vs thickness (number of MLs). Resistance vs thickness from 3 to 6 ML is shown in the inset.

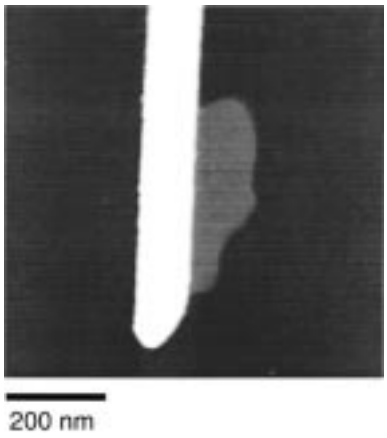

Figure 8. AFM height image of a 3 ML crystal that grew off of an Au nanowire on an SiO_2 substrate.

where R_c is the resistance associated with the metallurgical tip−Au contact, ρ is the Au resistivity (2.35×10^{-8} Ω m), l is the electron mean free path in Au (40 nm), and a_c is the radius of the contact area. At 50 nN loading force, we measured R_c = 20 Ω for a Au-coated tip in contact with Au, yielding a contact radius a_c = 4.5 nm and (assuming a circular contact) a contact area of ∼60 nm^2. This 60 nm^2 figure is somewhat larger than previous estimates of tip−sample contact areas based on adhesion measurements (10 nm^2).[13] However, in the adhesion-based calculations, the contact area was estimated at pull-off, i.e., when a tensile load was applied to the tip. Our relatively large 50 nN compressive load means that the contact area should be bigger than the adhesion estimate. Also, our contact resistance-based calculation assumes that there is no tunneling

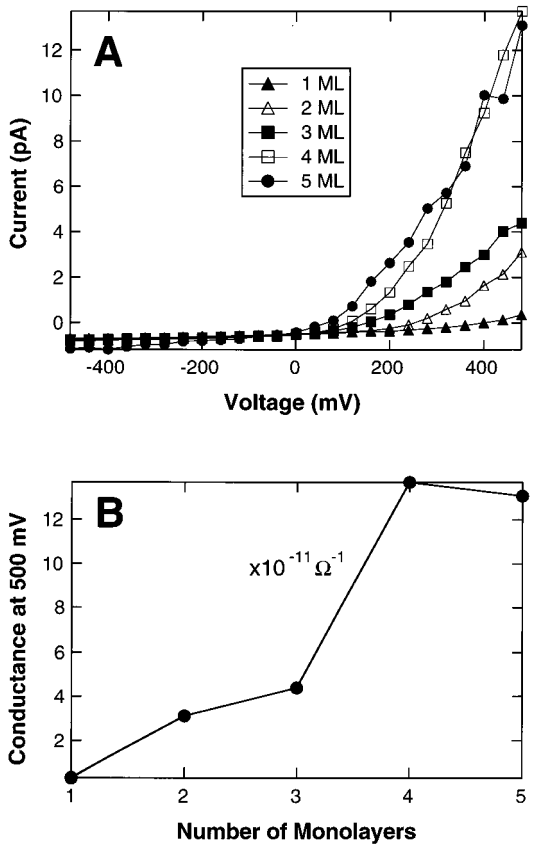

Figure 9. (A) Point contact $I-V$ characteristics of 6T crystals on SiO_2. Experimental configuration shown in Scheme 1D. (B) Horizontal conductance at 500 mV bias vs thickness (number of MLs). For an ohmic material, the conductance would be expected to increase with increasing thickness, eventually leveling off due to spreading resistance near the point contact.

of electrons outside the area of metallurgical contact. If tunneling is occurring, then R_c of the metallurgical contact is actually bigger than calculated, meaning the contact area is smaller than 60 nm^2.

With respect to structural characterization of the 6T crystals by AFM, we found no evidence of changes in lattice parameters, step heights, or overall morphologies of the crystals after exposure to iodine for 30 min. Iodine is known to intercalate between layers of thiophene oligomers,[11] and so expansion of the 6T lattice along the a axis certainly could be expected. However, from the conductance data shown in Figure 7 and the geometry of the point contact measurements, we calculate that the dopant concentration in the crystals we studied is no greater than one part per thousand.[14] That concentration corresponds to approximately one dopant molecule for every 400 nm^2, assuming the dopant is spread evenly across a single 6T layer, and it is very unlikely that structural changes associated with such doping levels are detectable by AFM, though the electrical conductivity increases by orders of magnitude. Conductance measurements at various points across the surface of crystals (e.g., Figure 5) gave no convincing evidence that the dopant was not uniformly distributed. In light of the estimated dopant concentration, it is completely reasonable that we observed no structural changes upon 30 min exposure of the crystals to iodine.

The most striking result of our transport studies on 6T is the conductance versus crystallite thickness plot for the vertical measurements, Figure 7B, which shows a peak in conductance at 3 ML. The conductance of a classic ohmic material scales

inversely with thickness. To the extent that the doped 6T crystals behave ohmically, one expects monotonically decreasing conductance with increasing 6T crystal thickness, with 1 ML crystals showing the highest conductance. In fact, we observe that the 1 ML crystals are the least conductive of the crystals we tested, and 2 ML crystals are only slightly better. For crystals 3 ML and thicker, the conductance does indeed scale inversely with thickness. This is seen best in the inset to Figure 7B, which shows a nearly linear relationship between resistance (reciprocal of conductance) and 3−6 ML thickness. Since the conductance of these thicker crystals appears to follow the classical model, the challenge is to explain the low conductance of the 1 and 2 ML crystals, realizing that conduction in the thicker crystals implies that charge in fact *can* be transported through the first and second 6T layers nearest the metal substrate.

Two principle mechanisms by which charge could travel across the 1 and 2 ML crystals are direct tip-to-substrate tunneling and 6T-facilitated transport, the latter consisting of hole injection into 6T, hole migration within the crystal, and exiting of holes at the second metal contact. The low conductance of the 1 and 2 ML crystals means that neither tunneling nor 6T-facilitated transport is occurring appreciably. The absence of significant tunneling current can be rationalized by comparison of our experiments with recent tunneling spectroscopy measurements on individual C_{60} molecules.[8a,d] In those measurements, C_{60} was found to enhance (relative to vacuum) the tunneling current through the tip−substrate junction by 6 orders of magnitude. However, the tunneling current still depended exponentially on the tip−substrate separation. At 50 mV bias, 1 pA was obtained at 15 Å tip−substrate separation. Since in our experiments, the thickness of 1 6T ML is 23 Å, the tunneling currents at 50 mV through 1 ML crystals are likely to be smaller than 1 pA and even smaller for 2 ML crystals. In fact, we observe that conductance through 2 ML crystals is slightly *greater* than conductance through 1 layer, supporting the conclusion that a direct tunneling mechanism is not important.

There are several possible reasons for poor conduction via the second mechanism, 6T-facilitated transport. One is that the 1 and 2 ML crystals are not doped effectively by iodine. Doping with iodine changes the conductance of 6T crystals by orders of magnitude, and if 1 and 2 ML crystals have relatively low dopant concentrations, their conductances will naturally be much lower than the conductances of the 3−6 ML crystals. However, while 1 ML crystals *might* have low dopant concentrations,[15] it is difficult to explain why the dopant concentration in 2 ML crystals would be less than in the 3−6 ML crystals. Without an unambiguous method for determining the iodine concentration in the crystals, we cannot rigorously exclude the possibility that low dopant concentration is the cause for low conductance of 1 and 2 ML crystals.

An alternative explanation is that the 1 and 2 ML crystals could be a different crystallographic polymorph having inherently lower conductivity. Our AFM measurements show that the height of the 1 and 2 ML crystals corresponds to one- and two-layer step heights observed on thicker (3−6 ML) crystals, indicating that the 6T molecules in the thin crystals are oriented similarly to those in the thicker crystals. However, we could not acquire sufficiently good molecular resolution images on these thin crystals to determine the lattice parameters accurately, which opens the possibility that the lattice parameters are not precisely the same as the 3−6 ML crystals. A possible consequence of this is that the *horizontal* (in-plane) conductivity could

SCHEME 2: Electronic Energy Level Diagram Showing 6T HOMO and LUMO States and the Fermi Levels of the Au Contacts. HOMO−LUMO Separation Is Smaller for the Doped 6T States

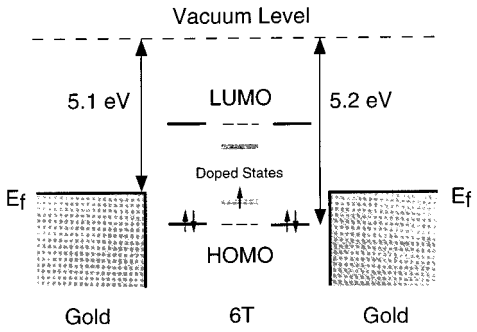

be lower in the 1 and 2 ML crystals than in the 3−6 ML crystals. The horizontal conductivity of the crystals may be important to conduction through the crystal thickness (vertical direction), since spreading the charge over the entire crystal could effectively increase the cross sectional area available to transport charge. If this is the case, a polymorph that has lower lateral conductivity may show lower conductance in the vertical CPAFM measurements.[16]

It is also likely that there is an intrinsic barrier to hole injection at Au−6T (or Au/S−6T) interfaces. Indeed, the data in Figure 7B are consistent with the interpretation that it is difficult to inject charge into any 6T layer that is in direct contact with Au. Both 1 and 2 ML crystals show low conductance relative to the thicker crystals, and in these cases each 6T layer touches at least one metal electrode. If holes cannot be inserted easily from the electrodes into the 1 and 2 ML crystals, the overall conductance of these crystals will be low. Understanding of the origin of a barrier, if it exists, will require detailed electronic structure calculations, but generally speaking it is already well-known that a mismatch between a molecular HOMO (or the narrow band derived from interacting HOMOs) and a metal Fermi level leads to a built-in potential barrier to hole injection across metal−organic interfaces.[17]

If the reason for the low conductance of 1 and 2 ML crystals is a barrier to charge injection, it is worth commenting on how injection into thicker crystals is possibly any easier. Scheme 2 shows an energy level diagram depicting the HOMO and LUMO levels of 6T and the Fermi levels of the Au contacts. Also shown in the scheme are midgap doped 6T states that result from I_2 oxidation of 6T molecules not in contact with either electrode.[18] We have drawn undoped 6T energy levels adjacent to the Au contacts to suggest that these states are pinned (undopable) due to interaction with the Au contacts. We postulate that holes could be injected from Au contacts directly into the doped 6T states. Such a process could be facilitated by the fact that the doped states lie closer to the Au Fermi level. However, with this reasoning the challenge is to explain why a two-step process, i.e., tunneling across one 6T layer into the crystal with subsequent tunneling across a second 6T layer into the second metal contact, is easier than direct tunneling from tip to substrate across 1 ML. It appears that one must postulate further that once charge is injected, there is delocalization of charge onto the 6T layers adjacent to the contacts, facilitating tunneling.

It is currently not possible for us to establish conclusively which of the above explanations accounts for the low conductance of the 1 and 2 ML crystals. Other potential explanations also exist, such as dependence of transport on compressive stress

generated by the tip.[8a] What we can conclude is that we have observed nonohmic transport in these extremely thin 6T crystallites, underscoring the fundamental importance of further investigations of nanoscale electrical transport in organic crystals.

Importantly, the horizontal $I-V$ characteristics of the 6T crystallites on SiO_2 support the interpretation that a barrier at Au−6T interfaces exists. In these measurements, the tip was 100 nm away from the second Au contact (as opposed to 2−14 nm away in the vertical measurements), and to obtain measurable currents, we swept the voltage from −500 to +500 mV. Figure 9A shows that for crystals of different thicknesses we observe strongly rectifying $I-V$ traces; current flows only when the tip is biased positively. Since rectification would not be observed if there were no charge injection barriers (ohmic contacts), we can conclude that (1) there is a hole injection barrier at each of the Au−6T contacts, and (2) holes may breach this barrier only at the extremely small tip−6T contact where the electric fields are very strong. 6T is a hole conductor, and holes must be injected into the crystal from a positively biased contact in order for current to flow. The majority of the applied voltage is always dropped across the tip−6T contact (it has much larger resistance), and it is therefore reasonable that injection of holes from the positively biased tip occurs at much lower voltage than when the nanowire is positively biased.

We do not observe rectifying behavior over the ±50 mV regime in the vertical measurements presumably because the fields across the crystals in these experiments are much larger, meaning the barriers at both contacts can be modulated. However, to the extent that the low conductances of the 1 and 2 ML crystals in the vertical measurements are a result of poor charge injection, we can conclude that both the vertical and horizontal conductance experiments show evidence of a potential barrier associated with Au−6T contacts.

The thickness dependence of the conductance in the horizontal measurements, Figure 9B, is distinctly different than in the vertical conductance measurements. We observe that the conductance increases with thickness until four layers, at which it plateaus. In a classical picture, current would be expected to increase with thickness since thicker crystals have a larger cross sectional area available for transport, but the increases would level off on account of spreading resistance near the tip contact. Therefore, the observed trend is consistent with expectations. Importantly, the relatively low conductance of the 1 and 2 ML crystals is expected in these experiments. Details of the thickness dependence of the conductance depend on the electric field structure and dopant concentration near the tip, and therefore we can only speculate that the large increase in conductance from 3 to 4 ML is due to an increase in the rate of charge injection. Once the charge is injected into a 6T layer, the structural anisotropy of the crystal prevents the charge from spreading easily into other layers, which implies that after a certain critical thickness (e.g., 4 ML) conduction would not depend heavily on thickness because the charge is transported in only one or two layers.[19]

In summary, we have demonstrated that CPAFM may be applied successfully to measuring the electrical transport properties of extremely thin crystallites of sexithiophene over nanoscopic length scales. To make these measurements, we have modified an AFM so that we can image samples in tapping mode and record current−voltage characteristics in contact, which greatly enhances the feasibility of the measurements by reducing damage to the tip and sample. We have shown that the conductance of the crystallites is strongly dependent on dopant concentration and has unusual dependence on crystallite thickness. The combination of imaging and electrical characterization afforded by CPAFM will make it a powerful tool for correlating nanoscale structure with transport properties in organic materials.

Acknowledgment. C.D.F. thanks the NSF (DMR-9624154-001) and the University of Minnesota for support of this work. E.L.G. thanks the Department of Defense for a National Defense Science and Engineering Graduate Fellowship.

References and Notes

(1) Epstein, A. J.; Yang, Y. *MRS Bulletin* **1997**, *22*, 13.

(2) (a) Gutman, F.; Lyons, L. E. *Organic Semiconductors*; Wiley: New York, 1967. (b) Pope, M.; Swenberg, C. E. *Electronic Processes in Organic Crystals*; Clarendon Press: New York, 1982. (c) Silinsh, E. A.; Capek, V. *Organic Molecular Crystals*; AIP Press: New York, 1994. (d) Greenham, N. C.; Friend, R. H. In *Solid State Physics*; Ehrenreich, H., Spaepen, F., Eds.; Academic Press: New York, 1995; Vol. 49.

(3) Forrest, S. R. *Chem. Rev.* **1997**, *97*, 1793.

(4) (a) Foxman, E. B.; McEuen, P. L.; Meirav, U.; Wingreen, N. S.; Meir, Y.; Belk, P. A.; Belk, N. R.; Kastner, M. A. *Phys. Rev. B* **1993**, *47*, 10020. (b) Ashoori, R. C.; Stormer, H. L.; Weiner, J. S.; Pfeiffer, L. N.; Pearton, S. J.; Baldwin, K. W.; West, K. W. *Phys. Rev. Lett.* **1992**, *69*, 1592. (c) Su, B.; Goldman, V. J.; Cunningham, J. E. *Science* **1992**, *255*, 313. (d) Reed, M. A.; Randall, J. N.; Aggarwal, R. J.; Matyi, R. J.; Moore, T. M.; Wetsel, A. E. *Phys. Rev. Lett.* **1988**, *60*, 535.

(5) Dai, H.; Wong, E. W.; Lieber, C. M. *Science* **1996**, *272*, 523.

(6) Tanimoto, M.; Kanisawa, K.; Shinohara, M. *Jpn. J. Appl. Phys.* **1996**, *35*, 1154.

(7) Thomson, R. E.; Moreland, J. *J. Vac. Sci. Technol. B* **1995**, *13*, 1123.

(8) For STM transport measurements on single molecules: (a) Joachim, C.; Gimzewski, J. K. *Chem. Phys. Lett.* **1997**, *265*, 353. (b) Bumm, L. A.; Arnold, J. J.; Cygan, M. T.; Dunbar, T. D.; Burgin, T. P.; Jones, L., II; Allara, D. L.; Tour, J. M.; Weiss, P. S. *Science* **1996**, *271*, 1705. (c) Andres, R. P.; Bein, T.; Dorogi, M.; Feng, S.; Henderson, J. I.; Kubiak, C. P.; Mahoney, W.; Oshifchin, R. G.; Reifenberger, R. *Science* **1996**, *272*, 1323. (d) Joachim, C.; Vinuesa, J. F. *Europhys. Lett.* **1996**, *33*, 635. (e) Joachim, C.; Gimzewski, J. K.; Schlittler, R. R.; Chavy, C. *Phys. Rev. Lett.* **1995**, *74*, 2102. (f) Eigler, D. M.; Schweizer, E. K. *Nature* **1990**, *344*, 524.

(9) (a) Torsi, L.; Dodabalapur, A.; Rothberg, L. J.; Fung, A. W. P.; Katz, H. E. *Science* **1996**, *272*, 1462. (b) Lovinger, A. J.; Rothberg, L. J. *J. Mater. Res.* **1996**, *11*, 1581. (c) Garnier, F.; Horowitz, G.; Fichou, D.; Yassar, A. *Synth. Met.* **1996**, *81*, 163. (d) Dodabalapur, A.; Katz, H. E.; Torsi, L.; Haddon, R. C. *Science* **1995**, *269*, 1560. (e) Dodabalapur, A.; Torsi, L.; Katz, H. E. *Science* **1995**, *268*, 270. (f) Lovinger, A. J.; Davis, D. D.; Ruel, R.; Torsi, L.; Dodabalapur, A.; Katz, H. E. *J. Mater. Res.* **1995**, *10*, 2958. (g) Katz, H. E.; Dodabalapur, A.; Torsi, L.; Lovinger, A. J.; Ruel, R. *Proc. Am. Chem. Soc. Div. Polym. Mater. Sci. Eng.* **1995**, *72*, 467. (h) Horowitz, G.; Bachet, B.; Yassar, A.; Lang, P.; Demanze, F.; Fave, J.-L.; Garnier, F. *Chem. Mater.* **1995**, *7*, 1337. (i) Garnier, F.; Hajlaoui, R.; Yassar, A.; Srivastava, P. *Science* **1994**, *265*, 1684. (j) Garnier, F.; Yassar, A.; Hajlaoui, R.; Horowitz, G.; Deloffre, F. *Electrochim. Acta* **1994**, *39*, 1339. (k) Garnier, F.; Yassar, A.; Hajlaoui, R.; Horowitz, G.; Deloffre, F.; Servet, B.; Ries, S.; Alnot, P. *J. Am. Chem. Soc.* **1993**, *115*, 8716. (l) Horowitz, G.; Peng, X.; Fichou, D.; Garnier, F. *J. Appl. Phys.* **1990**, *67*, 528. (m) Horowitz, G.; Fichou, D.; Peng, X.; Xu, Z.; Garnier, F. *Solid State Comm.* **1989**, *72*, 381.

(10) (a) Hegner, M.; Wagner, P.; Semenza, G. *Surf. Sci.* **1993**, *291*, 39. (b) Wagner, P.; Hegner, M.; Guntherodt, H. J.; Semenza, G. *Langmuir* **1995**, *11*, 3867.

(11) Hotta, S.; Waragai, K. *J. Mater. Chem.* **1991**, *1*, 835.

(12) Loiacono, M. J.; Frisbie, C. D. Unpublished results.

(13) Noy, A.; Frisbie, C. D.; Rosznyai, L. F.; Wrighton, M. S.; Lieber, C. M. *J. Am. Chem. Soc.* **1995**, *117*, 7943.

(14) From Figure 7, conductance (G) is no higher than 10^{-9} Ω^{-1}. This maximum value corresponds to conductivity ($\sigma = GL/A$) of 10^{-3} Ω^{-1} cm^{-1} using 60 nm^2 as the contact area and $L = 10$ nm. Hole concentration, p, is derived from $\sigma = p\mu e$, where μ is the hole mobility and e is the fundamental charge. μ was taken to be 0.01 cm^2 V^{-1} s^{-1}, a low estimate based on the literature,[9] giving $p = 10^{18}$ cm^{-3} or about 10^4 holes per 1 μm × 1 μm × 10 nm 6T crystal. In a crystal of this size, there are 10^7 6T molecules, so the concentration of dopant is ∼1 ppt.

(15) Iodine is known to intercalate between layers in lamellar oligothiophene crystals (see ref 11). Therefore, it may be that the dopant cannot penetrate 1 ML crystals.

(16) The importance of horizontal conductivity in the vertical measurements may be determined by examining the dependence of vertical conductance on crystallite area. We compared conductances of crystals with nearly the same area to ensure that the differences in conductance we measured were not the consequence of large differences in crystal area.

(17) (a) Garnier, F.; Kouki, F.; Hajlaoui, R.; Horowitz, G. *MRS Bulletin* **1997**, June, 52. (b) Parker, I. D. *J. Appl. Phys.* **1994**, *75*, 1656.

(18) Taliani, C.; Blinov, L. M. *Adv. Mater.* **1996**, *8*, 353.

(19) Due to poor π orbital overlap along the *a* direction (Scheme 1A), hole mobility is much greater in the *bc* plane of 6T crystals (see ref 9c).